MODELING DIMETHYLSULPHIDE PRODUCTION AT THE BERMUDA ATLANTIC TIME SERIES (BATS)

Roger A. Cropp[1], John Norbury[2], Albert J. Gabric[1] and Roger D. Braddock[1].
[1] Faculty of Environmental Sciences, Griffith University, Nathan, Queensland, Australia.
[2] Mathematical Institute, University of Oxford, Oxford OX3 9DU, UK

ABSTRACT

Dimethylsulphide (DMS) is produced by upper ocean ecosystems and emitted to the atmosphere where it may have an important role in climate regulation. Several attempts to quantify the role of DMS in climate change have been undertaken in modeling studies. We examine a model of biogenic DMS production and describe its endogenous dynamics and sensitivities. We extend the model to develop a one-dimensional version that more accurately resolves the important processes of the mixed layer in determining the ecosystem dynamics. Comparisons of the results of the one-dimensional model with vertical profiles of DMS in the upper ocean measured at the Bermuda Atlantic Time Series suggest that the model represents the interaction between the biological and physical processes well. Our analysis of the model confirms its veracity and provides insights into the important processes determining DMS concentration in the oceans.

KEY WORDS

Dimethylsulphide, biogeochemical modeling, one-dimensional model.

1. Introduction

Dimethylsulphide (DMS) is produced by marine ecosystems from its precursor dimethyl-sulphoniopropionate (DMSP). DMSP is abundant in phytoplankton and present in sufficient concentration to sustain a net flux of DMS to the atmosphere. Once emitted to the atmosphere DMS is oxidised to form non-sea-salt sulphate and methanesulphonate aerosols. Shaw [1] and later Charlson et al. [2] postulated that DMS-producing phytoplankton could stabilise global climate. This has led to a focus on the role of upper ocean ecosystems in shaping climate [3].

The vertical physical dynamics of the mixed layer are a critical driving force determining ecosystem dynamics in the upper ocean [4]; by comparison, horizontal advection is believed to have little influence on mixed layer ecosystems [5]. The mean irradiance field, controlled by the interaction of light penetration and the mixed layer depth, and the supply of nutrients into the mixed layer are important limiting factors on biological production [6]. Phytoplankton blooms in the ocean occur after a deepening of the mixed layer brings new nutrient to surface waters and subsequent stratification of the surface waters traps phytoplankton in a relatively highly illuminated, high-nutrient regime, providing ideal conditions for the initiation of a phytoplankton bloom [7]. Shallowing of surface mixed layers also contributes to enhancing DMS production by initiating phytoplankton succession toward stronger DMSP producers, allowing a higher efficiency of conversion from DMSP to DMS, and by possibly inhibiting bacterial consumption of DMS [8].

Here we examine the dynamical properties of the Gabric et al. [9] model, hereafter referred to as the GMSK model. The depth-averaged GMSK model can, to some extent, include the influence of variations in mixed layer depth, as it averages over the mixed layer, but it cannot resolve or explain structures such as sub-surface chlorophyll maxima commonly observed in oceans [7]. One-dimensional ecosystem models resolve these effects much more accurately, and reveal the influence of exogenous physical forcings on the dynamics of the models more clearly.

We extend the GMSK model to resolve the vertical structure of the ocean, and note the effect of the inclusion of the physical dimension on the model dynamics. The one-dimensional model is forced by seasonal changes in mixed layer depth, sea surface temperature, photosynthetically available radiation and sea surface wind speed. We compare the one-dimensional model with vertical profiles of DMS measured as part of the Bermuda Atlantic Time Series (BATS) [10]. In contrast to the approach taken by Lefevre et al. [11] we do not vary the parameters temporally to obtain the best fit but calibrate a reduced parameter set to reproduce the BATS data. We calibrated eight of the parameters so that the slope of the regression line, linking model predicted

DMS with the DMS concentrations measured at BATS, was approximately unity.

2. The GMSK Model

The equations of state of the GMSK model are given by equations (1) to (7) [9].

$$\frac{dP}{dt} = k_{23}F\left(R,T\right)\left(\frac{N}{N+k_{24}}\right)P - k_1\left(\frac{P}{P+k_2}\right)B - k_4PZ \tag{1}$$

$$\frac{dB}{dt} = k_1\left(1-k_{11}\right)\left(\frac{P}{P+k_2}\right)B - k_8\left(\frac{B}{B+k_9}\right)F - k_{10}B + k_{25}\left(1-k_{11}\right)\left(\frac{N}{N+k_{26}}\right)B \tag{2}$$

$$\frac{dF}{dt} = k_8\left(1-k_{14}\right)\left(\frac{B}{B+k_9}\right)F - k_{13}F\,, \tag{3}$$

$$\frac{dZ}{dt} = k_4\left(1-k_{20}\right)PZ - k_{19}Z\,, \tag{4}$$

$$\frac{dN}{dt} = k_{10}B + k_{11}\left[k_{25}\left(\frac{N}{N+k_{26}}\right)B + k_1\left(\frac{P}{P+k_2}\right)B\right] + k_{13}F + k_8k_{14}\left(\frac{B}{B+k_9}\right)F + k_{19}Z + k_4k_{20}PZ - k_{23}\left(\frac{N}{N+k_{24}}\right)P - k_{25}\left(\frac{N}{N+k_{26}}\right)B, \tag{5}$$

$$\frac{dDMSP}{dt} = k_5k_{33}P + k_{21}k_{33}Z - k_{27}DMSP - k_{31}DMSP\,, \tag{6}$$

$$\frac{dDMS}{dt} = k_6k_{33}P + k_{27}DMSP - k_{28}DMS - k_{29}DMS - k_{30}DMS\,. \tag{7}$$

In these equations *P* represents phytoplankton, *B* bacteria, *F* flagellates, *Z* zooplankton, *N* nutrient, *DMSP* the concentration of DMSP and *DMS* the concentration of DMS. The *P, B, F, Z* and *N* quantities are expressed as concentrations of atomic nitrogen (mg N m^{-2}) and *DMSP* and *DMS*. as concentrations of atomic sulphur (mg S m^{-2}). The k_i are fixed parameters measured by [12]. The model averages over the mixed layer and all concentrations and parameter values are scaled by the depth of the mixed layer.

The GMSK model equations were scaled by a characteristic time (k_{23}) that corresponds to the maximum growth rate of the phytoplankton. Equations (1)-(5) are scaled by the characteristic concentration of the total nitrogen mass, *No*, and equations (6) and (7) by the characteristic total sulphur mass, *So*.

The GMSK model is essentially a nitrogen-based ecosystem model given by equations (1)-(5) with uni-directional coupling to a sulphur-based biochemical model given by equations (6) and (7).

The steady state *DMS* concentration of the sulphur model is given by:

$$DMS^* = \frac{P\left(k_5k_{27} + k_6k_{27} + k_6k_{31}\right) + k_{21}k_{27}Z}{\left(k_{27}+k_{31}\right)\left(k_{28}+k_{29}+k_{30}\right)}\,. \tag{8}$$

The stability of this point is given by the eigenvalues of the coefficient matrix of the *DMSP* and *DMS* equations of state. These eigenvalues are always negative, indicating that the critical point given by equation (8) is always an asymptotically stable node and the system will return to its equilibrium state rapidly after perturbation (ie it is highly resilient). The sulphur sub-model dynamics are therefore slaved to, and will closely follow, the dynamics of the ecosystem model, in particular the time evolution of *P* and *Z*.

Equation (8) denotes a linear relationship between *DMS* and *P* concentrations and is a similar form to the empirical relationship derived by Simo and Dachs [13]. As linear correlations between DMS and chlorophyll (a surrogate measure of *P*) have not been detected in analysis of global data sets [14], the influence of the zooplankton in equation (8) is important.

3. The One-Dimensional Model

The one-dimensional GMSK model is obtained from the depth-averaged GMSK model by resolving the distribution of concentrations and fluxes over depth in the water column and allowing diffusive and advective fluxes. The model equations are now reaction-diffusion equations of the type:

$$\frac{\partial C}{\partial t} = G - k_v \frac{\partial C}{\partial z} + \frac{\partial}{\partial z}\left(D \frac{\partial C}{\partial z} \right), \quad (9)$$

where C is a vector of P, B, F, Z, N, $DMSP$ and DMS concentrations, G is net production (growth – loss) given by equations (1)-(7), k_v is the vertical advection velocity (m/day) and D is vertical turbulent diffusivity (m^2/day) [3]. Note that when the production terms (G) in equation (9) are replaced by the right-hand-sides of equations (1)-(7) the emission term $k_{30}DMS$ is deleted from equation (7). The emission of DMS from the sea to the air is included in the one-dimensional model as a boundary condition at the sea-air interface rather than as a sink term in the production equations.

3.1. Boundary Conditions

The upper boundary of the model is formed by the sea surface and the lower boundary is set at 200 metres. The region of the water column below the mixed layer acts as a reservoir of nutrient that may be entrained into the mixed layer when it deepens. This scenario allows the model to reproduce the physical mechanisms that initiate phytoplankton blooms [7]. Sinking of phytoplankton is included in the model as this is reasonably well documented [15, 16], but vertical migration by zooplankton is not included as the effect of turbulence on zooplankton feeding is not clear [7]. Similarly the effect of sedimentation of DMS when adsorbed onto particles is insignificant compared to the flux to the atmosphere and has been ignored [17].

The boundary condition for equation (9) is given [18] by:

$$\left(1-\xi\right)k_v C - D\frac{\partial C}{\partial z} = 0, \quad (10)$$

where ξ is a parameter specifying the nature of the boundary. If $k_v \neq 0$ (ie for P only) a perfectly absorbing boundary is specified by $\xi = 1$, and a perfectly reflecting boundary is specified when $\xi = 0$. A mass-conservative ecosystem model accords with the findings of Spitz et al. [19] that some ecosystem models fit real data best if mass is approximately conserved. Zero-flux boundary conditions are therefore implemented for the state variables on both boundaries with the exception of P at the bottom boundary and DMS at the top boundary.

Phytoplankton sink through the water column and out of the upper, photic zone, and contribute to 'marine snow' that delivers nutrient to the deep ocean [15]. The bottom boundary condition for P therefore allows the sinking flux of phytoplankton to pass through it. The nutrient lost as phytoplankton is eventually replaced by processes such as upwellings associated with the divergence of the Ekman transport [20] that deliver inorganic nutrients back to the upper ocean. The mass falling through the bottom boundary is therefore uniformly reinjected into the sub-mixed layer as nutrient.

The Liss and Merlivat [21] model of gas transfer rate is used as a DMS boundary condition for the one-dimensional model:

$$F_{vent} = k_{tr} DMS\,. \quad (11)$$

The boundary condition for DMS at the top boundary is therefore the condition:

$$\frac{dDMS}{dz} = k_{tr} DMS\,. \quad (12)$$

The piston velocity (k_{tr}) is calculated from three equations representing different sea state / wind speed (w) scenarios. These are: a smooth surface regime (w = 0 - 3.6 m s^{-1}), a rough surface regime (w = 3.6 - 13 m s^{-1}) and a breaking wave regime (w > 13 m s^{-1}):

$$\begin{aligned} k_{tr} &= 0.17\alpha w, && w \le 3.6\ ms^{-1}, \\ k_{tr} &= \beta\left(2.85w - 10.3\right) + 0.6\alpha, && 3.6 < w \le 13\ ms^{-1}, \\ k_{tr} &= \beta\left(5.9w - 49.9\right) + 0.6\alpha, && w > 13\ ms^{-1}, \end{aligned} \quad (13)$$

where $\alpha = \left(\frac{600}{Sc}\right)^{2/3}$ and $\beta = \sqrt{\frac{600}{Sc}}$.

The dimensionless Schmidt number (Sc) is the ratio of the absolute viscosity of seawater to the diffusivity of DMS in water. For a given gas, the Schmidt number decreases with increasing water temperature. The dependence of Sc on sea surface temperature for DMS has been experimentally derived by Saltzman et al. [22]

$$\begin{aligned} Sc &= 2674.0 - 147.12 * SST \\ &\quad + 3.726 * SST^2 - 0.038 * SST^3 \end{aligned}. \quad (14)$$

3.2 Diffusion and Temperature Profiles

The diffusivity is a function of depth and includes uniform mixing in the mixed layer, the gradient in mixing strength that occurs at the pycnocline, and a uniform mixing profile in the sub-mixed layer. A sigmoid function (equation (15)) is used to generate a diffusivity profile for use in the model simulations:

$$D = \frac{D_{max} + D_{min} e^{r\left(D_{min} - D_{max}\right)\left(\frac{2\left[z - MLD\right]}{H}\right)}}{1 + e^{r\left(D_{min} - D_{max}\right)\left(\frac{2\left[z - MLD\right]}{H}\right)}}, \qquad (15)$$

where D is the diffusivity (m^2/day), D_{max} is the maximum mixed-layer diffusivity ($0 < D_{max} < \sim 1000$), D_{min} is the minimum sub-mixed layer diffusivity ($0 < D_{min} < \sim 10$) and z is the depth in the water column (m). The depth of the model domain is H (m) and MLD is the depth of the mixed layer (m). The quantity r (day/m^2) is a parameter that controls the steepness of the pycnocline ($1 < r < 50$), where $r \sim 20$ generates pycnoclines typical of those observed in the ocean. The use of this sigmoid function assumes homogeneity of all properties within the mixed layer, which is considered realistic except perhaps for conditions of deep convective mixing [23, 24].

An analogous function is used to describe the vertical temperature profile. The temperature of the mixed layer (T_{max}) is also assumed to be homogeneous and the sub-mixed layer temperature (T_{min}) is held constant. The vertical temperature profile is given by:

$$T = \frac{T_{max} + T_{min} e^{r\left(T_{min} - T_{max}\right)\left(\frac{2\left[z - MLD\right]}{H}\right)}}{1 + e^{r\left(T_{min} - T_{max}\right)\left(\frac{2\left[z - MLD\right]}{H}\right)}}. \qquad (16)$$

3.3. Forcings

The specific growth rate of phytoplankton in the one-dimensional GMSK model is subject to variation with depth due to changes in light intensity, represented by $F(R, T)$ in equation (1). The relationship described by Walsh et al [16], which includes the effects of self-shading, is used to describe light-limited P growth in this model:

$$R_L = \frac{I(z)}{I_S} e^{\left(1 - \frac{I(z)}{I_s}\right)}, \qquad (17)$$

where $I(z) = I_0 e^{-\left(k_w + k_p P\right)z}$, (18)

and k_w is the light attenuation of seawater, k_p is the light attenuation due to self-shading of phytoplankton, z is the depth in metres, I_0 is the incident surface irradiation (W/m^2) and I_s is the phytoplankton saturating irradiation (W/m^2).

Laboratory studies of phytoplankton have also revealed a dependence of phytoplankton growth rates on temperature [25, 26]. The temperature dependence of phytoplankton growth used in this model was estimated by Eppley [26] to be:

$$R_T = e^{0.063\left(T - T_{\max}\right)}, \qquad (19)$$

where T is the ambient temperature (^{0}C) and T_{max} is the maximum annual temperature.

The one-dimensional model equations are also scaled by characteristic concentrations: the total nitrogen mass (No) for the nitrogen-based equations and a characteristic sulphur mass (So) for the sulphur-based equations. A characteristic sulphur mass is selected so that $S_0 = k_{33} N_0$, and k_{33} (the phytoplankton sulphur as DMSP to nitrogen ratio) may be cancelled from the scaled sulphur equations. Depth is scaled by the simulation depth of the model, H, the maximum annual mixed layer diffusivity D_{max} and a characteristic time T_{char} is selected so that:

$$T_{char} = \frac{H^2}{D_{\max}}. \qquad (20)$$

The Method of Lines [27, 28] was used to solve the partial differential equations of the one-dimensional model.

4. Results

We compared the one-dimensional model with vertical profiles of DMS measured as part of the Bermuda Atlantic Time Series (BATS) [10]. The BATS data used in this analysis comprised 247 measurements of DMS taken in the top 100 metres of the water column on 27 days spaced at irregular intervals (1 – 33 days apart) over a twelve month period. DMS measurements were usually made at depths of 1, 5, 10, 15, 20, 30, 40, 60, 80 and 100 metres.

The model was integrated for 730 days, with the second 365 days (366 – 730) being used to compare with the BATS data. We used a genetic algorithm [29] to calibrate eight of the 33 model parameters to minimize the squared error between the model and BATS data at the 247 BATS data points. We also calibrated the phytoplankton sulphur (as DMSP) to nitrogen ratio so that the slope of the regression line linking the DMS concentration predicted by the model and the BATS DMS concentration was approximately unity. These parameters and their calibrated values are presented in Table 1.

Table 1: Parameter values tuned to fit BATS data.

PAR	PROCESS	UNITS	VALUE
k_4	Z grazing rate (per individual) on P	$m^3 mgN^{-1} d^{-1}$	0.0137
k_{19}	Z specific N excretion rate	d^{-1}	0.0177
k_{20}	Proportion of N uptake excreted by Z	-	0.8096
k_{23}	Maximum rate of N uptake by P	d^{-1}	0.2392
k_{29}	Maximum DMS photo-oxidation rate	d^{-1}	0.9267
k_{33}	Phytoplankton S(DMSP):N ratio	-	0.8000
k_v	Phytoplankton sinking velocity	md^{-1}	0.3559
I_s	Phytoplankton saturating irradiance	Wm^{-2}	71

The comparison of the one-dimensional model output with the BATS data is presented in Figure 1.

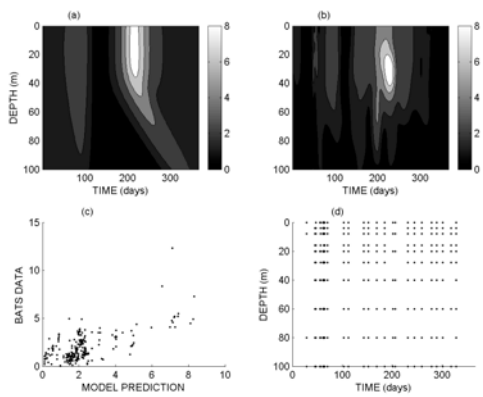

Figure 1: Comparison of time series of water column concentrations of DMS produced by the model with those measured at BATS: the depth-time distribution of DMS concentration produced by the model (a) and interpolated from the BATS data (b), scatter plot of BATS measurements and model predictions at same time and depth points (c) and depth-time location of BATS measurements (d). Contour lines are drawn at 1, 2, 4, 6 and 8 nM in panels (a) and (b).

The broad scale structures of Figures 1 (a) and (b) are quite similar, with both the model and data evidencing a broad, low concentration DMS peak at about day 80 - 100 and a clearly defined, high concentration DMS peak at about day 230. The large bloom occurs at a depth of 30 metres on day 232 in the BATS data, and at a depth of 24 metres on day 216 in the model predictions.

Comparisons of descriptive statistics of the model and measured data are presented in Table 2.

Table 2: Model predictions vs BATS data.

FEATURE	MODEL	BATS
Mean *DMS* conc (nM)	2.0	1.9
Std dev of *DMS* conc (nM)	1.7	1.5
Max *DMS* conc (nM)	8.9	12.3
Day of max *DMS* conc	216	232
Depth of max *DMS* conc (m)	24	30

The maximum in the BATS data is largely attributable to one data point with a very high concentration (approximately 7 standard deviations above the mean and 50% higher than the next highest concentration) on day 232. Due to the few data defining the maximum, and the paucity of data in the preceding 46 days, we elected not to calibrate the model to reproduce the timing exactly (although this was possible) but to improve the overall variation explained by the model. Figure 1 and Table 1 reveal that the model does a good job of reproducing the major characteristics of the BATS data. As the model only explains 44% of the variation in the data, it does not do a good job of reproducing the fine detail, but this is to be expected as the model uses a homogeneous mixed layer specified by equation (15) and does not resolve many of the factors that lead to fine scale variations in DMS concentration.

5. Discussion

Comparison of the calibrated one-dimensional model results with vertical profiles of DMS measured at BATS reveals that the model does a good job resolving spatial and temporal variations in DMS concentration. The model predicted the mean and standard deviation of the annual concentration of DMS accurately, as well as explaining up to 44% of the variation in the observed data. It also accurately predicted the timing and depth of major and minor peaks in DMS concentration, but underestimated the magnitude of the peaks. This may be in part due to the model using a homogeneous mixed layer that prevented it from resolving the finer detail of the spatial and temporal variation of the BATS data.

The multi-faceted approach employed in our evaluation of the GMSK model has provided insights into the important mechanisms in the model that would not have become evident if we had just evaluated the model's ability to reproduce observed data. These insights may provide useful information for the design of future field studies and may also provide an opportunity to rigorously test the process representation of the GMSK model.

6. Acknowledgements

The authors would like to thank the SeaWiFS Project (Code 970.2) and the Distributed Active Archive Centre (Code 902) at the Goddard Space Flight Centre, Greenbelt, MD 20771, for the production and distribution of the SeaWiFS data respectively. These activities are sponsored by NASA's Mission to Planet Earth Program (http://seawifs.gsfc.nasa.gov). The Advanced Very High Resolution Radiometer data was obtained from the NASA Physical Oceanography Distributed Active Archive Centre at the Jet Propulsion Laboratory / California Institute of Technology (http://podaac.jpl.nasa.gov). The mixed layer depth data were provided by the Carbon Dioxide Information Analysis Center, Oak Ridge National Laboratory, Tennessee (http://cdiac.ornl.gov/ftp/ ndp076).

References

[1].Shaw, G.E., Bio-controlled thermostasis involving the sulphur cycle. *Climate Change*, 5, 1983, 297-303.

[2].Charlson, R.J., et al., Oceanic phytoplankton, atmospheric sulphur, cloud albedo and climate. *Nature*, 326, 1987, 655-661.

[3].Gabric, A., et al., Modeling the biogeochemical cycle of dimethylsulfide in the upper ocean: A review. *Chemosphere - Global Change Science*, 3, 2001, 377-392.

[4].Eigenheer, A., W. Kuhn, and G. Radach, On the sensitivity of ecosystem box model simulations on mixed-layer depth estimates. *Deep-Sea Research I*, 43, 1996, 1011-1027.

[5].Denman, K.L. and M.A. Pena, A coupled 1-D biological/physical model of the northeast subarctic Pacific Ocean with iron limitation. *Deep-Sea Research II*, 46, 1999, 2877-2908.

[6].Doney, S.C., D.M. Glover, and R.G. Najjar, A new coupled, one-dimensional biological-physical model for the upper ocean: Applications to the JGOFS Bermuda Atlantic Time-series Study (BATS) site. *Deep-Sea Research II*, 43, 1996, 591-624.

[7].Mann, K.H. and J.R.N. Lazier, *Dynamics of Marine Ecosystems*. 2 ed, (Cambridge, Mass.: Blackwell Science, 1996).

[8].Simo, R. and C. Pedros-Alio, Role of vertical mixing in controlling the oceanic production of dimethyl sulphide. *Nature*, 402, 1999, 396-399.

[9].Gabric, A.J., et al., Modeling the production of dimethylsulfide during a phytoplankton bloom. *Journal of Geophysical Research*, 98, 1993, 22,805-22,816.

[10].Dacey, J.W.H., et al., Temporal variability of dimethylsulfide and dimethylsulfoniopropionate in the Sargasso Sea. *Deep-Sea Research*, 45, 1998, 2085-2104.

[11].Lefevre, M., et al., A model of dimethylsulfide dynamics for the subtropical North Atlantic. *Deep-Sea Research I*, 49, 2002, 2221-2239.

[12].Gabric, A.J., P.A. Matrai, and M. Vernet, Modelling the production and cycling of dimethylsulphide during the vernal bloom in the Barents Sea. *Tellus*, 51B, 1999, 919-937.

[13].Simo, R. and J. Dachs, Global ocean emission of dimethylsulfide predicted from biogeophysical data. *Global Biogeochemical Cycles*, 16, 2002, 26-1:26-10.

[14].Kettle, A.J. and others, A global database of sea surface dimethylsulfide (DMS) measurements and a procedure to predict sea surface DMS as a function of latitude, longitude and month. *Global Biogeochemical Cycles*, 13, 1999, 399-444.

[15].Smayda, T.J., The suspension and sinking of phytoplankton in the sea. *Oceanography and Marine Biology Annual Review*, 8, 1970, 353-414.

[16].Walsh, J., D.A. Dieterle, and J. Lenes, A numerical analysis of carbon dynamics of the Southern Ocean phytoplankton community: the roles of light and grazing in effecting both sequestration of atmospheric CO_2 and food availability to larval krill. *Deep-Sea Research I*, 48, 2001, 1-48.

[17].Jodwalis, C.M., R.L. Benner, and D.L. Eslinger, Modeling the dimethylsulfide ocean mixing, biological production, and sea-to-air flux for high latitudes. *Journal of Geophysical Research*, 105, 2000, 14,387-14,399.

[18].Gabric, A.J. and J. Parslow, Effect of physical factors on the vertical distribution of phytoplankton in eutrophic coastal waters. *Australian Journal of Marine and Freshwater Research*, 40, 1989, 559-569.

[19].Spitz, Y.H., J.R. Moisan, and M.R. Abbott, Configuring an ecosystem model using data from the Bermuda Atlantic Time Series (BATS). *Deep-Sea Research II*, 48, 2001, 1733-1768.

[20].Pond, S. and S.L. Pickard, *Introductory Dynamical Oceanography*. 2 ed, (Oxford: Butterworth-Heinemann, 2000).

[21].Liss, P.S. and L. Merlivat, *Air-sea gas exchange rates: Introduction and synthesis.*, in *The Role of Air-sea Exchange in Geochemical Cycling.*, P. Baut-Menard, Editor, (Reidel: Hingham, 1986).

[22].Saltzman, E.S., et al., Experimental determination of the diffusion coefficient of dimethylsulfide in water. *Journal of Geophysical Research*, 98, 1993, 16,481-16,486.

[23].Martin, P.J., *Testing and comparison of several mixed-layer models.*, Naval Ocean Research and Development Activity. 1986.

[24].Martin, P.J., Simulation of the mixed layer at OWS November and Papa with several models. *Journal of Geophysical Research*, 90, 1985, 903-916.

[25].Goldman, J.C. and E.L. Carter, A kinetic approach to the effect of temperature on algal growth. *Limnology and Oceanography*, 19, 1974, 756-766.

[26].Eppley, R.W., Temperature and phytoplankton growth in the sea. *Fishery Bulletin*, 70, 1972, 1063-1085.

[27].Schiesser, W.E., *Computational Mathematics in Engineering and Applied Science*, (Boca Raton: CRC Press, 1994).

[28].Schiesser, W.E., *The Numerical Method of Lines: Integration of Partial Differential Equations.*, (San Diego: Academic Press, 1991).

[29].Holland, J.H., *Adaptation in natural and artificial systems.*, (Ann Arbour: University of Michigan Press, 1975).